Studies in Applied Electromagnetics and Mechanics

Series Editors: K. Miya, A.J. Moses, Y. Uchikawa, A. Bossavit, R. Collins, T. Honma, G.A. Maugin, F.C. Moon, G. Rubinacci, H. Troger and S.-A. Zhou

Volume 24

Previously published in this series:

Vol. 23. F. Kojima, T. Takagi, S.S. Udpa and J. Pávó (Eds.), Electromagnetic Nondestructive Evaluation (VI)
Vol. 22. A. Krawczyk and S. Wiak (Eds.), Electromagnetic Fields in Electrical Engineering
Vol. 21. J. Pávó, G. Vértesy, T. Takagi and S.S. Udpa (Eds.), Electromagnetic Nondestructive Evaluation (V)
Vol. 20. Z. Haznadar and Ž. Štih, Electromagnetic Fields, Waves and Numerical Methods
Vol. 19. J.S. Yang and G.A. Maugin (Eds.), Mechanics of Electromagnetic Materials and Structures
Vol. 18. P. Di Barba and A. Savini (Eds.), Non-Linear Electromagnetic Systems
Vol. 17. S.S. Udpa, T. Takagi, J. Pavo and R. Albanese (Eds.), Electromagnetic Nondestructive Evaluation (IV)
Vol. 16. H. Tsuboi and I. Vajda (Eds.), Applied Electromagnetics and Computational Technology II
Vol. 15. D. Lesselier and A. Razek (Eds.), Electromagnetic Nondestructive Evaluation (III)
Vol. 14. R. Albanese, G. Rubinacci, T. Takagi and S.S. Udpa (Eds.), Electromagnetic Nondestructive Evaluation (II)
Vol. 13. V. Kose and J. Sievert (Eds.), Non-Linear Electromagnetic Systems
Vol. 12. T. Takagi, J.R. Bowler and Y. Yoshida (Eds.), Electromagnetic Nondestructive Evaluation
Vol. 11. H. Tsuboi and I. Sebestyen (Eds.), Applied Electromagnetics and Computational Technology
Vol. 10. A.J. Moses and A. Basak (Eds.), Nonlinear Electromagnetic Systems
Vol. 9. T. Honma (Ed.), Advanced Computational Electromagnetics
Vol. 8. R. Collins, W.D. Dover, J.R. Bowler and K. Miya (Eds.), Nondestructive Testing of Materials
Vol. 7. C. Baumgartner, L. Deecke, G. Stroink and S.J. Williamson (Eds.), Biomagnetism: Fundamental Research and Clinical Applications

Volumes 1-6 were published by Elsevier Science under the series title "Elsevier Studies in Applied Electromagnetics in Materials".

ISSN 1383-7281

Electromagnetic Nondestructive Evaluation (VIII)

Edited by

Thierry Sollier
CEA-LIST, Gif-sur-Yvette, France

Denis Prémel
CEA-LIST, Gif-sur-Yvette, France

and

Dominique Lesselier
L2S-DRE, CNRS-SUPELEC-UPS, Gif-sur-Yvette, France

IOS Press

Amsterdam • Berlin • Oxford • Tokyo • Washington, DC

1) The choice of the measurement system parameters can be guided by the dimension of the uncertainty ranges. The measurements with a poor efficiency should be avoided in favour of others with higher effectiveness. "Specialised" measurements for the detection of particular parameters can be included, if necessary.

2) The uncertainty ranges due to the system parameters **q** help to identify the critical aspects of the detection system and of the computing model, to which particular attention should be paid, whereas other aspects, with less influence on system performance, can be treated more coarsely.

3) The introduction of the modified OF, defined as a statistical average, can improve the identification ability in presence of noise or uncertainties but heavily increases the computational burden of the solving procedure: therefore the adoption of a high performance parallel computing environment becomes mandatory.

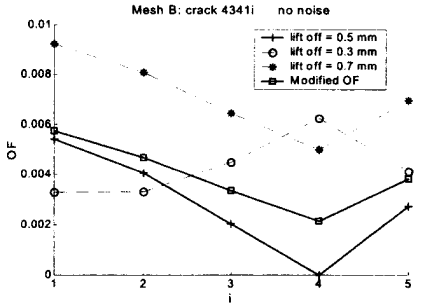

Figure 7. OF dependence by the crack depth for different coil lift-off and modified OF for a *4341i*-type crack.

Acknowledgements

This work has been partly sponsored by Italian Education and Research Ministry (MIUR) in the framework of the Relevant National Interest Research Project "MADEND".
The authors want to thank R. Albanese and G. Rubinacci for the use of the Cariddi code for the present work.

References

[1] Skordev, A., "Uncertainties and errors in Non-Destructive Characterisation of Discontinuities", *Proc. of 15th WCNDT*, Roma, Italy, October 15-21, 2000, http://www.ndt.net/article/wcndt00/toc/rel.htm.
[2] Pairazaman, C., Keller, S., and Rummel, W.D., "Reliability Assurance for Automated Eddy Current Inspection Systems", *Proc. of 15th WCNDT*, Roma, Italy, October 15-21, 2000, http://www.ndt.net/article/wcndt00/toc/rel.htm.
[3] Ericsson, L., and Stepinski, T., "Robust Signal Processing for Material Noise Suppression in Ultrasonic NDT", *Rev. of Progress in QNDE*, vol. 12A, 1993, pp. 695-702.
[4] Albanese, R., and Rubinacci, G., "Finite Element Methods for the Solution of 3D Eddy Current Problems" in *Advances in Imaging and Electron Physics*, Academic Press, vol. 102, 1998.
[5] Cioffi, M., Formisano, A., and Martone, R., "Analysis of Concurrent Multi-Frequency Eddy Current Testing Data", *Proc. of ENDE 02*, Saarbrücken, Germany, June 13-14, 2002.
[6] Jung, D.H., and Lee, B.C., "Development of a simple and efficient method for robust optimisation", *Int. J. Numerical Methods in Engineering*, vol. 53, issue 9, March 2002, pp. 2201-2215.
[7] Yoon, S.B., Jung, I.S., and Hyun, D.S., "Robust Shape Optimization of Electromechanical Devices", *IEEE Trans. on Magnetics*, vol. 35, n. 3, May 1999, pp. 1710-1713.
[8] Alotto, P., Magele, C., Renhart, W., Steiner, G., and Weber, A., "Robust Target Function in Electromagnetic Design", *Compel*, vol. 22, n. 3, 2003, pp. 549-560.
[9] Cioffi, M., Formisano, A., and Martone, R., "Increasing Design Robustness in Evolutionary Optimisation", *Proc. of PMAPS 2002*, Napoli, Italy, September 2002, to be published on *Compel*.

Electromagnetic Nondestructive Evaluation (VIII)
T. Sollier et al. (Eds.)
IOS Press, 2004

Numerical Modelling of Eddy Current Non-Destructive Evaluation by Integral Formulation and Parallel Implementation*

Ermanno CARDELLI, Antonio FABA
Department of Industrial Engineering, University of Perugia, Perugia, Italy.
Raffaele FRESA, Salvatore VENTRE
DIFA, University of Basilicata, Potenza, Italy. DAEIMI University of Cassino, Cassino, Italy.

Abstract. In this paper we present some results drawn from a research project of national interest named MADEND (Methods and Applications of Non-destructive Electromagnetic Diagnostic). In particular we show a comparison between two numerical models: eddy current integral formulation on parallel computer systems and differential formulation of finite element method. The numerical results and accuracy are confirmed by experimental tests.

1. Introduction

In Italy, since January 2002, some University research groups have been working on a so called "Project of Remarkable National Interest" of the National Italian Ministry of Education about methods and applications of electromagnetic diagnostic based on eddy current phenomena. The name of the project is MADEND and its purpose is to present and to develop the research possibilities in this field. Some results dealing with the MADEND programme are reported in this paper. In particular we present here a numerical model based on integral formulation and parallel implementation that allows a great saving of calculation time with respect to traditional numerical models. The benchmarks defined for this comparison are the MADEND benchmarks # 1, 2 and 3. The benchmark #1 is an aluminium plate with a thickness of 4 mm. On this plate there is an artificial defect with cylindrical shape, with a diameter of 1 mm and a height of 4 mm, (reduced respectively to 3mm and 2 mm for the benchmarks #2 and #3). The used probe is a coil placed on the metallic surface under test. For the benchmark # 2 and 3 the probe coil is placed on the opposite side with respect to the cylindrical defect. This coil is electrically linked to a suitable balanced bridge circuit and the voltage variation on the bridge allows the crack identification.

2. Integral formulation and parallel implementation

Integral formulation

The design and the analysis phases of modern devices for engineering applications, including among others the electromagnetic non-destructive evaluation, require accurate numerical solutions of Maxwell equations in the Quasi Stationary Magnetic limit. In the last decades many scientists focused their research activity on this topic. In the usual classification the

* This work has been supported by the Italian Ministry of Education (MIUR, Project MADEND) and EURATOM/ENEA/CREATE.

proposed approaches are divided in the two categories of integral and differential formulations.

The integral approaches present several advantages with respect to the differential ones because they require only the discretization of the space domain where the sources and the materials are located; moreover the regularity conditions at infinity for unbounded domains are implicitly included in the formulation, so that the overall discretization cost is very limited. Moving parts can be easily taken into account, while the presence of non linear magnetic materials require an additional moderate effort.

For linear materials, the numerical model is given by a system of linear algebraic equations with a dense coefficient matrix. In this paragraph we recall the salient points of the formulation adopted for the development of Cariddi, a volume integral code intensively used in the sector of the nuclear fusion for the solution of 3D eddy current problems in the time or in the frequency domain [1].

From the mathematical point of view the code solves the Maxwell equations in the QSM limit.

With reference to the time domain formulation and adopting the usual formalism, let's assume that an impressed current density is present in the domain V_s and the fixed conducting domain V_c is characterized by the $\mathbf{E} = \eta\mathbf{J}$ constitutive relationship with the normal component of current density equal to zero on the boundary ∂V_c.

Posing $\mathbf{B} = \nabla \times \mathbf{A}$ and $\mathbf{E} = -\frac{\partial \mathbf{A}}{\partial t} - \nabla\varphi$, the solenoidality of the flux density $\mathbf{B}$ and the Faraday law are automatically imposed. Moreover, the vector potential $\mathbf{A}$ can be expressed in terms of both impressed and unknown current density sources as:

$$\mathbf{A}(\mathbf{r},t) = \frac{\mu_0}{4\pi}\int_{V_c}\frac{\mathbf{J}(\mathbf{r}',t)}{|\mathbf{r}-\mathbf{r}'|}dV' + \frac{\mu_0}{4\pi}\int_{V_s}\frac{\mathbf{J}_s(\mathbf{r}',t)}{|\mathbf{r}-\mathbf{r}'|}dV' = \frac{\mu_0}{4\pi}\int_{V_c}\frac{\mathbf{J}(\mathbf{r}',t)}{|\mathbf{r}-\mathbf{r}'|}dV' + \mathbf{A}_s(\mathbf{r},t) \quad (1)$$

The Ohm law can be satisfied in weak form finding $\mathbf{J} \in Q$ such that $\int_{V_c}(\eta\mathbf{J}-\mathbf{E})\cdot\mathbf{w}\,dV = 0$ with $\mathbf{w} \in Q$, where $Q = \{\mathbf{q} \in L^2_{div}(V_c) \,|\, \nabla\cdot\mathbf{q} = 0, \hat{\mathbf{n}}\cdot\mathbf{q} = 0 \text{ on } \partial V_c\}$ is the functional space of admissible solutions $\mathbf{q}$ and $\mathbf{L}^2_{div}(V_c) = \{\mathbf{a} \in \mathbf{L}^2(V_c) \,|\, \nabla\cdot q \in L^2(V_c)\}$.

The position $\nabla\times\mathbf{T}=\mathbf{J}$, where $\mathbf{T}$ is the electric vector potential, assures the solenoidality of $\mathbf{J}$ and the continuity of its normal component. Finally, we obtain:

$$\frac{\mu_0}{4\pi}\int_{V_c}\int_{V_c}\frac{\partial(\nabla\times\mathbf{T}(\mathbf{r}',t))/\partial t\cdot\mathbf{w}(\mathbf{r})}{|\mathbf{r}-\mathbf{r}'|}dV'dV + \int_{V_c}\eta(\nabla\times\mathbf{T}(\mathbf{r}',t))\cdot\mathbf{w}\,dV + \int_{V_c}\nabla\varphi\cdot\mathbf{w}\,dV = -\int_{V_c}\frac{\partial\mathbf{A}_s}{\partial t}\cdot\mathbf{w}\,dV \quad (2)$$

Since $\mathbf{J}, \mathbf{w} \in Q$ in V_c, results $\int_{V_c}\nabla\varphi\cdot\mathbf{w}\,dV = -\int_{\partial V_c}\varphi\,\mathbf{w}\cdot\hat{\mathbf{n}}\,dV = 0$

Furthermore, the electric vector potential can be expanded in terms of the basis functions $\mathbf{N}_k$ associated to the edges of the domain mesh : $\mathbf{T}(\mathbf{r},t) = \sum_{k=1}^{n} I_k(t)\mathbf{N}_k(\mathbf{r})$.

The boundary condition $\mathbf{J}\cdot\hat{\mathbf{n}} = 0$ on ∂V_c can be directly imposed on the weight functions $\mathbf{w}_k$, while their solenoidality can be automatically obtained by choosing $\mathbf{w}_k = \nabla \times \mathbf{N}_k$. In order to assure the uniqueness of the solution, the decomposition tree-cotree of the edges of the mesh is applied and only the basis functions associated with the edges of the cotree are retained as unknowns. In conclusion, the eq. (2) becomes:

$$\underline{\underline{L}}\frac{d\underline{I}}{dt} + \underline{\underline{R}}\underline{I} = \underline{V} \quad (3)$$

where $\underline{\underline{R}}$ is a sparse positive semidefinite symmetric matrix, while $\underline{\underline{L}}$ is a dense N×N symmetric positive definite matrix:

$$R_{i,j} = \int_{V_c}\eta\mathbf{w}_i\cdot\mathbf{w}_j\,dV \;;\; L_{i,j} = \frac{\mu_0}{4\pi}\int_{V_c}\int_{V_c}\frac{\mathbf{w}_i(\mathbf{r}')\cdot\mathbf{w}_j(\mathbf{r})}{|\mathbf{r}-\mathbf{r}'|}dV'dV \;;\; V_i = -\int_{V_c}\frac{\partial\mathbf{A}_s}{\partial t}\cdot\mathbf{w}_i\,dV \quad (4)$$

Adopting the theta time-stepping method for the time integration, the differential system (3) can be reduced to a linear algebraic system:

$$\underline{\underline{A}}\underline{I}(t_{k+1}) = \underline{\underline{B}}\underline{I}(t_k) + \theta\underline{V}(t_{k+1}) + (1-\theta)\underline{V}(t_k) \quad (5)$$

where $\underline{\underline{A}} = \frac{1}{\Delta t}\underline{\underline{L}} + \theta\underline{\underline{R}}$; $\underline{\underline{B}} = \frac{1}{\Delta t}\underline{\underline{L}} - (1-\theta)\underline{\underline{R}}$.

The formulation can also be developed in the frequency domain, leading to the complex linear algebraic system [1]:

$$\underline{\underline{Z}}\underline{I} = \underline{V} \quad (6) \qquad \text{where } \underline{\underline{Z}} = j\omega\underline{\underline{L}} + \underline{\underline{R}}$$

Parallel implementation

The implementation of Cariddi requires several tasks to be carried out :

1) Preprocessing (for instance, initialization and computation of the incidence matrices)
2) Computation of matrices $\underline{\underline{L}}$ and $\underline{\underline{R}}$ and vector $\underline{V}$, by means of volume integration
3) LU decomposition of the $\underline{\underline{A}}$ and Z matrices respectively for the solutions in time (eq. 5) and frequency (eq. 6) domains.
4) Computation of the solutions in time or frequency domain by back-substitution
5) Postprocessing (for instance, computation of integral quantities of interest like power, energy, etc)

The number of unknowns, N, used to discretize conductors and sources, affects the accuracy of the numerical solution. If N is increased to improve the accuracy, the memory occupation scales as $O(N^2)$, while the computational cost scales in a different way according to the nature of the task. The fast scaling of memory and CPU-time requirements set a severe limit on the maximum value of N that can be considered on standard Pcs. In alternative to the utilization of supercomputers, the parallel implementation of the code represents a convenient way to overcome the above mentioned limitations and to obtain accurate solutions by meshes with finer discretization.

Among the various steps required from the algorithm, for large values of N, the most critical ones in terms of CPU time are related to the computation of the $\underline{\underline{L}}$ matrix and to the LU decomposition operations: a simple analysis shows that they scale with the unknown number N respectively like $O(N^2)$ and $O(N^3)$. As ScaLAPACK libraries allow to perform the latter task in a very efficient way, we'll dedicate the remaining part of this section to illustrate shortly the algorithms proposed in [2] for the numerical computation of the matrix elements L_{ij} on a parallel computation system.

We recall that :

$$L_{ij} = \sum_{e_1 \in E_i} \sum_{e_2 \in E_j} \sum_{G_1=1,N_G} \sum_{G_2=1,N_G} \mathbf{w}_i(\mathbf{r}_{G_1}) \cdot \mathbf{w}_j(\mathbf{r}_{G_2}) J_{e_1}(\mathbf{r}_{G_1}) J_{e_2}(\mathbf{r}_{G_2}) / |\mathbf{r}_{G_1} - \mathbf{r}_{G_2}| \quad (7)$$

where E_i is the set of elements that share the edge i, J_{ei} is the Jacobian of the element e, computed at the Gauss point r_{Gi} and N_G is the number of Gauss points.

The direct use of this definition leads to a lack of efficiency because the inner loops over the elements have to be repeated several times, as each element contributes up to twelve unknowns. The redundancy can be avoided by subdividing the computation by elements on the different processors. On the other side, the above strategy imposes a cost in terms of communication overhead, because the contribution to a single matrix element is due to volume elements allocated on different processors.

These considerations lead to the following algorithm (Local Computation And Communication, LCAC).

1) **Initialization**

To obtain the best performances, the available processors, in a number equal to the square of an integer number, are allocated in a square grid. The matrix coefficients are partitioned between the processors in a two-dimensional block cyclic way [2].

On the other side the volume elements of the mesh are distributed by rows among different processors in order to have balanced loads and taking into account the symmetry of interaction among the elements. Pointers from rows of the local part of the L matrix to the same rows of the global L matrix and vice-versa are computed. Let's note that the same element L_{ij} can be present in different processors, since the edges i and/or j can belong to elements stored in different processors. In addition, for this reason, the memory required for storing the computed data could be, for some processors, much larger than the memory necessary for storing the local part of L.

2) **Computation of local matrices**

```
For each element of current_process Iel1 do
    for each element Iel2 with Iel2 ≥ Iel1 do
        Compute the edge-edge interactions associated to the couple of
        elements (iel1-iel2) taking into account the symmetry of the matrix,
        using indirect addressing.
    end for
end for
```

3) **Redistribution of local matrices**

The local contributions to the processors are summed according to the allocation of the unknowns required by the solver.

The last step requires an all-to-all communication among the processors that can become a bottle neck if the speed of the network is not very high. To obviate this situation we proposed a second algorithm (Local Algorithm, LA), that minimizes the data communication cost, by limiting it to the exchange of the data between processors at symmetrical positions in the processor grid; the price to be paid is a redundancy in the computation phase. On the other side, differently from what happens for the LCAC algorithm, the memory required for each processor is now exclusively related to the size of the local part of L.

In [2] it 's also showed that a suitable renumbering of the unknowns increases in general the computational efficiency.

The proposed algorithms have been implemented on a "beowulf system" (BWS) (consisting of a cluster of sixteen Pcs with a Pentium III 450 MHz CPU, 512Mb Ram, 8 GB EIDE hard disk, connected via a 16 port fast ethernet switch) and a "shared memory system", (i.e.a Sun Fire 880, equipped with 4 Ultra Sparc-3 750Mhz CPU, 12 Gb Ram, 100GB SCSI hard disk). The executed benchmarks showed a speed-up of 10 or 8 (respectively for complex or real systems) on the16 processors Beowulf system and of 3.3 or 3.6 (respectively for complex or real systems) on the 4 processors SUN workstation.

The LA algorithm performs better than LCAC on BWS because of the low communication speed. Instead, on the shared memory system SUN, the time devoted to communications is much shorter and the two algorithms show almost the same speed-up.

3. Differential formulation of finite element method

The finite element analysis is widely used in resistance and reactance calculation [3][4]. In this work we have used a differential formulation and two kind of unknowns: magnetic vector potential on the total region, and the electric scalar potential only inside the metallic plate (eddy current region). The basic equations are:

$$\nabla \times \left[\frac{1}{\mu}\right] \nabla \times \mathbf{A} + [\sigma] \frac{\partial \mathbf{A}}{\partial t} + [\sigma] \nabla \cdot \mathrm{V} = 0 \quad (1)$$

$$\nabla \cdot \left(-[\sigma] \frac{\partial \mathbf{A}}{\partial t} - [\sigma] \nabla \cdot \mathrm{V} \right) = 0 \quad (2)$$

$$\nabla \times \left[\frac{1}{\mu}\right] \nabla \times \mathbf{A} = \mathbf{J} \quad (3)$$

where **A** is the magnetic vector potential, V is the electric scalar potential and **J** the applied source current density vector. The basic algebraic equation shape is:

$$[\mathrm{B}]\{\dot{\mathbf{u}}\} + [\mathrm{C}]\{\mathbf{u}\} = \{\mathbf{J}\} \quad (4)$$

where $[\mathrm{B}]$ and $[\mathrm{C}]$ are a suitable coefficient matrix that takes into account the element shape functions, $\{\mathrm{u}\}$ is the vector of the unknowns (magnetic vector potential **A** and electric scalar potential V) and $\{\mathbf{J}\}$ is the vector of applied loads [5]. We have modeled the probe coil, the metallic plate as well as the empty space around them using a mesh of hexahedrons nodal elements. We have obtained meshes using an extruding technique that produces automatically a three-dimensional mesh from the two-dimensional map of the system constituted by the coil and the plate with the defect (see figure 1). In order to show clearly the used mesh type the figure 3 is limited to the region around the defect and the probe. The equivalent resistance and equivalent reactance of the system constituted by the probe coil and the plate with the defect are obtained by computing the current density and the magnetic vector potential. The current density has been evaluated in the center of the hexahedrons, while the magnetic vector potential in the center of the element has been derived by interpolating the values in the nodes. We have obtained satisfactory results using a cylindrical symmetry mesh centered in the probe coil (see figure 1). In order to avoid an excessively time-consuming re-meshing, it is necessary that different locations of the probe coil with respect to the crack can be modeled with the same grid or some parts of

it, suitably connected. In this case we have solved the problem simply by moving the crack on different positions with respect to the plate mesh, while the position of the probe coil was fixed. The position of the crack is determined by the material assignment (air or metal) for each volume cell, along the search path. The boundary conditions used are $\mathbf{A} = 0$ in a region with cylindrical shape and with a thickness up to ten times larger than the probe coil diameter. We have stopped the increasing of the diameter of the bounding region when we have attained no changes in the numerical solution.

4. Experimental set-up

The detection technique based on the impedance variation of a probe coil is well known, and widely studied and used for many applications. In particular it is possible to detect a thin crack in a metallic body by indirect measurement of the impedance variation of a probe coil, using the electrical circuit represented in figure 2. V is an a.c. voltage source, R is a bridge resistance, Z1 is the impedance of a probe coil placed on a metallic plate, Z2 is the impedance of a reference coil. The probe coil has 400 turns, 10 mm of height, 12 mm of inner diameter, 18 mm of outer diameter and 0.5 mm of average lift-off. The reference coil is identical to the probe coil described above, and is placed in a region of the metallic plate without defects. The value of Z2 is the same of Z1 when the probe coil is far from the defect position. This way, by moving the probe coil on the metallic plate surface and by measuring the voltage V_{BC} between the nodes B and C, it is possible to determine the defect locations in the metallic plate (see figure 2). This particular topology of electric circuit gives an output signal V_{BC} immune with respect to the change of the voltage source value and to the thermal phenomena of the probe coil.

Critical points for the experimental procedure are the positioning system for the probe coil with respect to the cracks on the metallic plate and the parameter acquisition system. We have faced these questions with the experimental set-up including a two-dimension automatic positioning system with a resolution of 0.1 mm, a signal voltage analyzer with a resolution of 1 μV for the VBC measurement, an amplified signal generator for the electrical circuit supply and dedicated software + digital control. This experimental set-up is represented in figure 3:

1 Automatic positioning system.
2 Signal voltage analyzer.
3 Signal generator.
4 Dedicate software + personal computer control for 1 and 2.

In particular the probe coil path and the acquisition time of each point of measure can be computer-controlled.

In our work we have analyzed three kinds of artificial defects realized on an aluminum plate. Shapes and dimension of these defects are represented in the figure 4. In the case b) and c) the probe coil is placed on the opposite side with respect to the cylindrical defect.

5. Numerical and experimental results

When the probe coil is placed on a given point around the defect, the voltage variation on the balanced bridge is calculated by means of both the integral formulation above and a classical differential formulation of finite element method. The results obtained and the

experimental data [6] are compared in the figures 5, 6 and 7. Some details about the cited numerical models, calculation time and computers used are reported in the table 1. It can be noted that the integral formulation on parallel systems gives more accurate results with reduced calculation time in relation to the classical finite element approach.

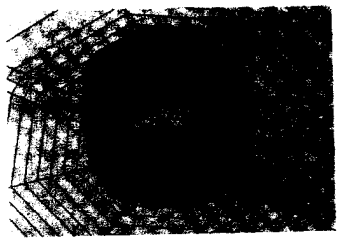

Fig. 1. Detail of probe coil + plate mesh.

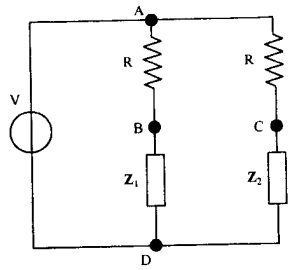

Fig. 2. Electrical circuit linked to probe coil.

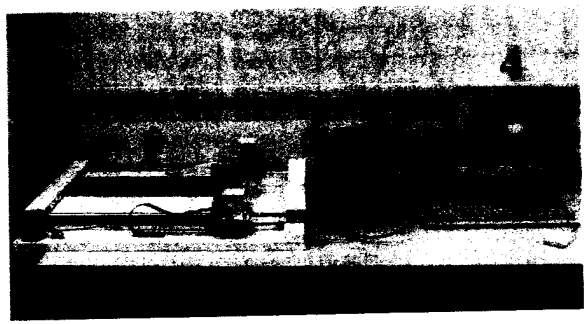

Fig. 3. Picture of experimental set-up.

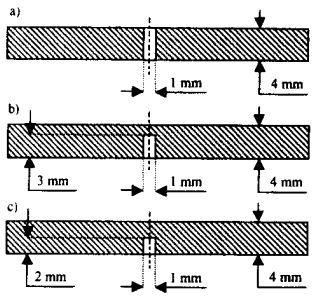

Fig. 4. Shape and dimension of defects.

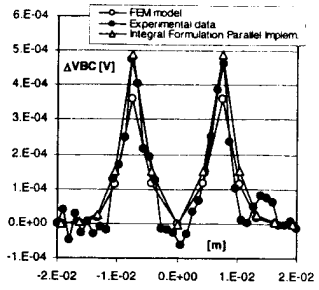

Fig. 5. Comparison between numerical and experimental data for defect a) described in figure 4.

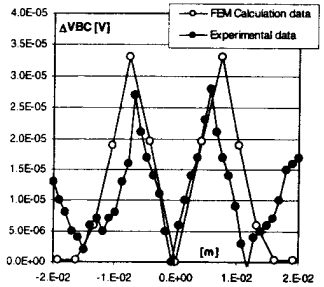

Fig. 6. Comparison between numerical and experimental data for defect b) described in figure 4.

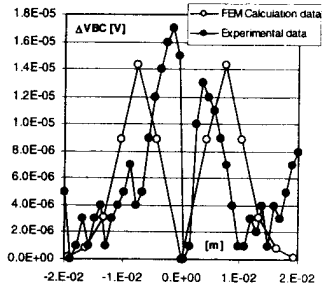

Fig. 7. Comparison between numerical and experimental data for defect c) described in figure 4.

Table 1: Numerical model performances and hardware details.

Numerical method	Number of elements	Calculation time results of fig. 1 [min]	Processor [MHz]	RAM Memory [Mb]	Hard Disk Memory [Gb]
Eddy current integral formulation on 16 nodes parallel systems	4224	164	Intel Pentium III© 450 (for each node)	512 (for each node)	8 (for each node)
Differential formulation of finite element method	6194	630	Intel Pentium III© 450	128	4

References

[1] R. Albanese, G. Rubinacci, "Finite element methods for the solution of 3D eddy current problems," *Advances in Imaging and Electron Physics*, vol. 102, pp. 1-86, 1998

[2] R. Fresa, G. Rubinacci and S. Ventre, "An eddy current integral formulation on parallel computer system", submitted for publication on the International Journal for Numerical Methods in Engineering.

[3] E. Cardelli, A. Faba, A. Massinelli, "FEM Applied to the Detection of Extremely Thin Cracks via Eddy Current Non Destructive Test", The 8th Joint MMM – Intermag Conference 2001, San Antonio, Texas, USA January 7 – 11, 2001.

[4] P. Burrascano, E. Cardelli, A. Faba, S. Fiori, A. Massinelli, "Numerical Analysis of Eddy Current Non-Destructive Testing (JSAEM Benchmark, Problem #6 – Cracks with different shapes)", Proc. of the E'NDE Conference, pp. 333 – 340, Budapest, Hungary, June 28 – 30, 2000.

[5] O. Biro and K. Preis, " On The Use of The Magnetic Vector Potential in the Finite Element Analysis of Three-Dimensional Eddy Currents", IEEE transactions on Magnetics, Vol. 25, No. 4, pp 3145-3159 (July 1989).

[6] E. Cardelli and A. Faba "FEM Analysis of Thin Cracks in Metallic Plates", Accepted for presentation to ISEM Conference, Versailles, Paris 2003.

[7] Rubinacci G., Tamburrino A., Villone F. Circuits/Fields Coupling and Multiply Connected Domains in Integral Formulations. IEEE Transactions on Magnetics 2002; 38: 581 –584.